

Influence of temperature fields on the processing of polymer powders by means of laser and mask sintering technology

D. Rietzel*, M. Drexler*, F. Kühnlein*, and D. Drummer*

*Institute of Polymer Technology, Friedrich-Alexander- University Erlangen-Nürnberg, Germany

REVIEWED, August 17 2011

Abstract

Besides their high potential for individual series-production, powder and beam based additive manufacturing technologies, like laser and mask sintering, are in general still restricted to prototyping applications. This is a result of multiple limitations concerning part properties (e.g. mechanical and geometrical), their insufficient reproducibility due to transient thermal conditions and the limited range of available materials. The main focal point of this paper is to show the influencing parameters (e.g. temperature fields in the building chamber) of powder-based thermoplastic processing technologies on part properties, like porosity and surface quality, and on the processability of further new polymers (e.g. polypropylene and polyoxymethylene).

1. Introduction

The properties of laser sintered parts, e.g. density, surface topography, accuracy of detail and dimension are determined by process parameters interacting with the material. In investigations, it was revealed, for instance, that the geometry of particles is a decisive factor that substantially determines component coarseness [1-2]. The size distribution and geometry of particles are of major importance for sintered parts' porosity. On the one hand, high powder density leads to higher part density, dimensional accuracy and strength in the sintered parts, yet it may deteriorate flowabilities on the other hand. Commercially available laser sintering powders with good flowabilities consist in general of spherulite particles with a narrow size distribution of $d = 60 \mu\text{m}$, and with a low share of fine particles below $d = 10 \mu\text{m}$ [3].

Apart from material application, temperature control during building is of major significance for the part's profile of properties. For part density, a closed melt film is crucial, making it necessary for the powder material to have low melt viscosity. Due to their wide range of softening and the resulting possibility of achieving low component densities, as well as a high dimensional stability, amorphous thermoplastics are employed e.g. as lost cores in precision casting [3]. Thus, for direct part manufacturing, only semi-crystalline polymers are relevant at present. Semi-crystalline plastics, however, are heated to the point above glass transition temperature, close to the crystalline melting point, with the laser merely fusing the crystalline shares. Due to the high chain mobility, decrease in viscosity is much steeper after exceeding this narrow range of crystalline melting. [4-5] In an ideal case, the building process would lead to the model state of quasi-isotherm laser sintering, where melt and solid powder exist side by side. The building process is carried out in a sort of two-phase mixing state. The laser merely introduces the energy that is necessary for the material to exceed the point of phase transition. For the subsequent creation of a coalesce film and thus fully dense parts the melting viscosity and surface tension are just as significant as the before shown powder density and flowability of laser sintering powders [6-7]. Temperature increase in the surrounding powder bed should be as small as possible, here. Another requirement of this process, in terms of material properties is that: The plastic material's crystallization temperature should be clearly below the crystalline melting point. In case the initial melting temperature is exceeded, powders will start to melt, whereas, if temperature is below initial crystallization temperature, the plastic melt produced up to then will start to crystallize, causing shrinkage respectively curling. This type of shrinkage is typical for the first molten layers as they are in contact with surrounding powder. In general a steady state is achieved after some layers, but as the freedom of design gains an increasing importance, e.g. for implants or lightweight structures, the effect of temperature gradients in the part bed will become more important. In Figure 1 a laser sintered structure was investigated by means of microscopy. The transmitted polarized light image taken from a microtome cut of single struts shows a lack in layer bonding and a continuous warpage of layers. This effect will be major part of the investigation presented in this paper.

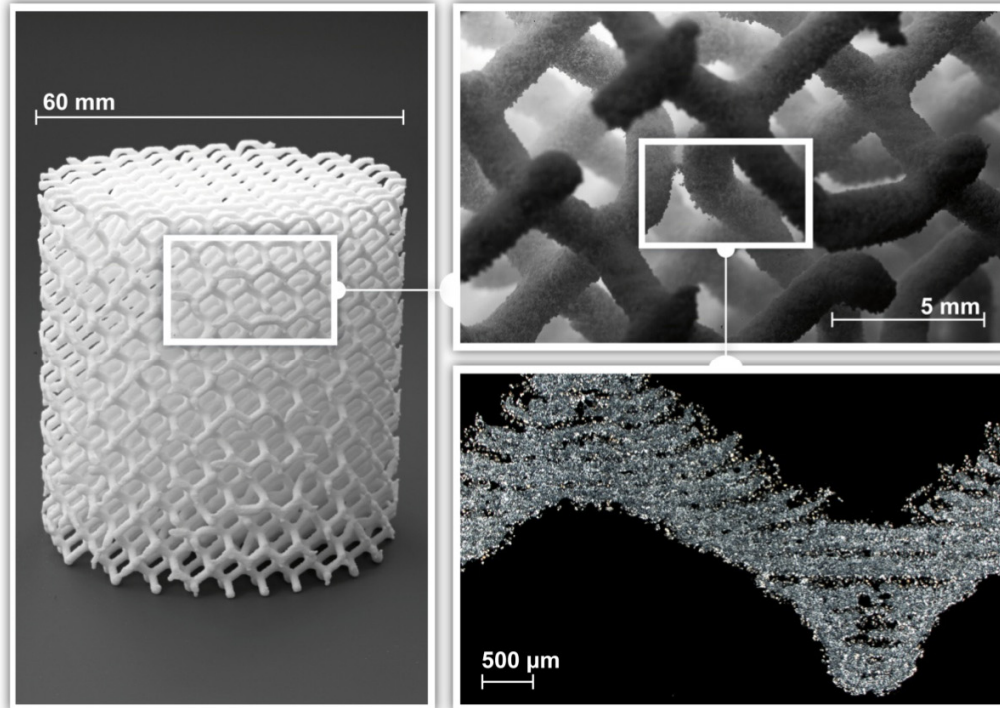


Figure 1: Microscopic investigation of a PA12, PA2200 SLS part

2. Materials and Methods

2.1 Materials and Powder Preparation

Commercially available laser sintering powder PA12 (PA2200, EOS GmbH) was tested as to its processing properties and compared to POM, PE-HD and PP powders. Generating spherulite particles directly from polymerization is not possible with all types of plastics. As an alternative, powders can be precipitated (e.g. PA12, PE-HD, PP) [8-9] or converted from pellets. Cryoscopic grinding is a well-proven method to make powder particles with a size less than 100 μm , as necessary for laser sintering. [10] The pellets are cooled down to $T_{\text{mill}} = -50\text{ }^{\circ}\text{C}$ in a cooling section and fed into a counter-rotating pinned disc mill (impact crusher principle). After milling, the powder is classified and screened down to a desired particle diameter. Cryoscopic grinding to a particle size below $d = 80\text{ }\mu\text{m}$ was done with POM. POM powder was mixed with 0.2 wt.-% of Aerosil[®], in order to step up flowability. In IR measurements conducted on PE-HD before, the material was found to have a high transmission coefficient when submitted to the wavelength of the used CO₂ laser ($\lambda = 10.6\text{ }\mu\text{m}$). [7] By adding 0.4 wt.-% of Carbon Black[®] the penetration depth of the laser could be limited to approximately 100 μm . As a result, the parts were black, had a high degree of absorption and better flowability.

2.2 Thermoanalytical Investigations

2.2.1 Time-dependent thermal analytic methods

To investigate the melting and crystallization behavior of PA12, PA2200 different thermoanalytical measurements were conducted. In order to define the melting and crystallization temperature DSC measurements are suitable. According to DIN 53765, 10 or 20 K/min is the standard heating and cooling rate, for thermoplastics. However laser sintering is a slow process of part generation, which makes standard measurement technologies unsuited to sufficiently describe the real process. In order to investigate the differences of cooling rates three different ones (10, 5 and 1 K/min) were chosen, too. In order to get more detailed information about the melting and solidification process, plate-plate rheometer tests were done with low frequency and slow heating/cooling rates of 1 K/min. The deformation in the oscillating test was 0.2 %.

Additionally pVT-measurements were carried out to analyze the volume change (v) of the sample under different pressures (p) and temperatures (T). The experimental system consists of a heated cylinder where different pressures can be applied by a plunger. In order to be able to extrapolate the findings for those measurements down to 1 bar several pressures (200, 400 and 800 bar) were provided under constant cooling rates of 3 K/min. The result gives an idea of the shrinkage of a sample from molten to solid state.

2.2.2 Isothermal methods

As those previous measurements are time-dependent the SLS process was also simulated by isothermal DSC measurements. The temperature is kept close to the crystalline melting point (T_{pm}) for a long period of time, and new preheated layers are applied on top of the previously sintered ones. The idea of quasi-isotherm laser sintering implements the assumption of melt which does not crystallize for a long period of time at a point just below its melting point. With crystallization related to time and temperature, DSC tests were carried out alongside the laser sintering process. The specimens were heated in a defined program to $T = T_{pm} + 20$ K at 20 K/min, cooled down to measurement temperature at a cooling rate of 40 K/min and kept in the isothermal state at different temperatures above the determined beginning of crystallization, as shown in [11]. The exothermal heat flows and crystallization times (the time between the beginning of the isothermal measurement t_0 and crystallization peak t_{pc}) were recorded. In a preprocessing the PA12 material was submitted to previous drying (in N_2) at 120 °C for 15 minutes in the DSC, since otherwise the results were not reproducible due to degradation and cross-linking. With the resulting DSC-curves crystallization times could be analyzed at different temperatures and the crystallization kinetics could be modeled. In general the crystallization process is split in 2 stages: primary and secondary crystallization process. For isothermal conditions the initial crystallization can be well described by the Avrami model. [12-13] The basis of the model hypothesizes that the relative crystallinity increases with the crystallization time t in following way:

$$X(t) = 1 - \exp(-kt^n) \quad (1)$$

In this case $X(t)$ is the weight fraction of crystallized material at time t , the Avrami coefficient k represents the crystallization rate and n is defined as the Avrami exponent. This equation can be described in following double logarithmic form:

$$\lg[-\ln(1-X(t))] = n \lg t + \lg k \quad (2)$$

By plotting $\lg[-\ln(1-X(t))]$ versus $\lg t$ the Avrami coefficients can be calculated from the slope of the linear portion and the intersection of the line with the ordinate. The calculation on the basis of the Avrami equation can lead to a model to describe the crystallization kinetics, but it is complicated and time-assuming. Thus according to an Arrhenius model, by Šesták and Berggren [14] another approach is provided to receive only the Activation Energy for a crystallization process. [11] Both methods were tested and the results were compared.

2.2.3 FEM Simulation

To transfer the findings of crystallization kinetics and the overall crystallization behavior of a polymer to the SLS conditions the cooling process and the thermal penetration after melting the powder was modeled and simulated by means of Finite Element Method. Therefore it is assumed that elements in the powder (Fig. 1, left) are heated to different temperatures by the insertion of different laser energies. Those elements also cool unequal after a line is scanned (Fig. 1, right), when different boundary conditions are defined. In order to find main influencing variables of the melting and cooling processes a DoE was constructed and the results were simulated. As basis for the standard parameters, values were taken from literature. [1, 7, 15-18] By means of minimum and maximum values the parameters are scaled by the factor of two. For better explanation the used parameters are illustrated in Table 1. The chosen laserpower of 5W (Factor -1) is based on standard parameters of a DTM Sinterstation 2000 where the experimental part was realized with. The particle diameter of 50 μm (+1) matches with the $d_{3,50}$ of PA12, PA2200. As minimum heat conductivity of 0,027 W/(mK) was measured

and the minimum absorbance was taken from literature [17]. In order to achieve evaluable results all parameters were doubled.

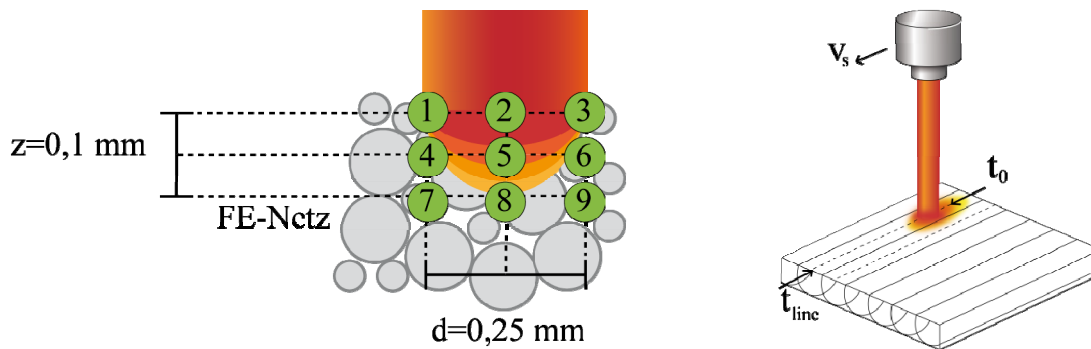


Fig. 1: Segmentation of the molten volume element (left) and investigated points in time

Parameter	Maximum (+1)	Minimum (-1)
Laserpower P_b	10 W	5 W
Heat source	Surface heat source	Volume heat source
Particle diameter	50 μm	25 μm
Heat conductivity	0,054 W/(mK)	0,027 W/(mK)
Absorbance	66 %	33 %
Absorbtion coefficient β (=1/ Particle diameter [4])	1/(25 μm)	1/(50 μm)

Table 1: Varied Parameters for the DoE

3 Results and Discussion

3.1 Thermoanalytical Investigations

By using different cooling rates for DSC measurements it could be shown that crystallization has a high time dependency. Fig. 2 (left) shows that crystallization starts at higher temperatures with lower supercooling of the molten material. The findings presented show that the investigated thermoplastics start to crystallize even before the assumed crystallization temperature is reached, when standard cooling rates of 10 or 20 K/min are used. The range of processing parameters, determined in the standard DSC process, are thus unsuited to serve as the sole processing criteria. The most important rheological result is the crossover point for melting ($T_{SP,m}$) and solidification ($T_{SP,c}$) respectively, Fig. 2 (left). It is noticeable that the flowing of the sample starts between the onset of the melting peak and the peak temperature derived by DSC measurements. In contrast to this result the solidification measured by a plate-plate rheometer is about 5-10 K below the crystallization peak temperature determined by DSC runs.

The additionally carried out pvT measurements on the other hand give an overview of the volume change while cooling. Especially while crystallization there is a step-up in the slope of the cooling curves. The total volume change $\Delta V_{\text{crystallization}}$ is about 29 % of the whole volume change during solidification to a temperature below glass transition. In view of having no pressure and no mould constraints that can affect solidification, possible temperature gradients are main influencing factors for the dimensional stability of parts.

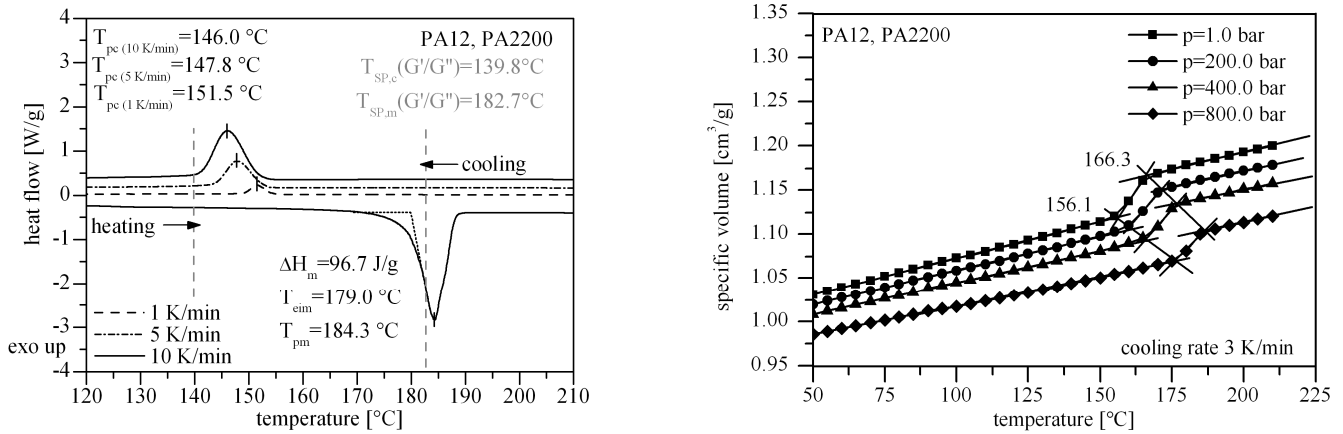


Fig. 2: Results of DSC, plate-plate rheometer and pvT measurements on PA12, PA2200

Due to the fact, that selective laser sintering is considered a very slow process in which the polymer is kept in a molten state for a long period of time; isothermal measurements were done to simulate an ongoing crystallization process. Besides the determination of the building temperature via the difference between crystallization and melting peak in temperature also the available time between phase changes can be measured for different isothermal temperatures by this method, Fig. 3 (left). Thus the time-stability of the two-phase area can be analyzed. On basis of the isothermal measurements at different temperatures the crystallization curves are mathematically integrated and double logarithmic plots of the converted material versus $\ln t$ are carried out. The resulting curves are linearized by a fit curve and their slope and the point of intersection with the y-axis are used as Avrami coefficient k and Avrami exponent n . The illustration in Fig. 3 (right) shows that the linear adjustment can be done between high conversion rates but is not accurate for higher temperatures anymore. Above 171°C there are several linear sections in the double logarithmic plot which is supposed to be due to the existence of a secondary crystallization caused by the impingement of PA12 spherulites. [19]

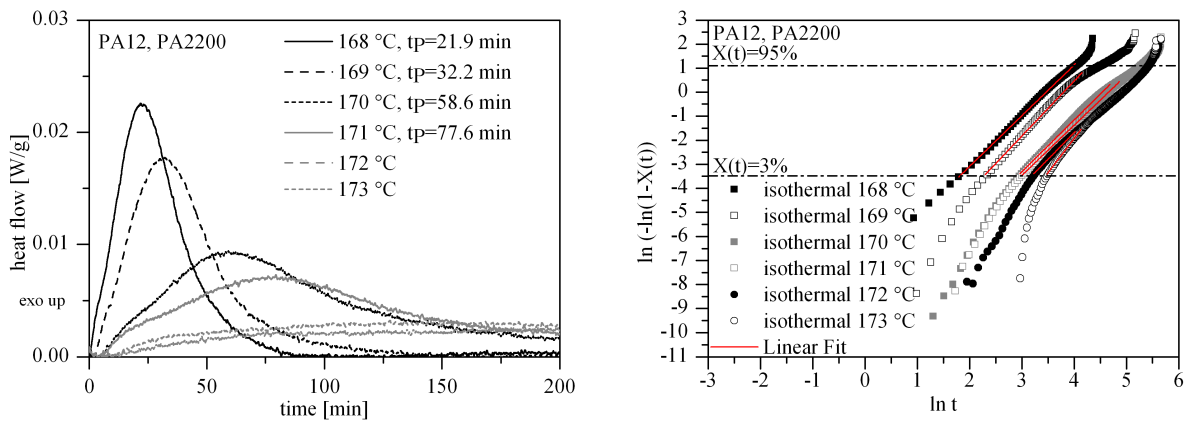


Fig. 3: Isothermal DSC heat flow curves at different temperatures near the crystallization temperatures (left) and double logarithmic plots out of the integrated curves

Subsequently the resulting coefficients are used to model the temperature dependent conversion curves and a comparison is done with measurements, Fig. 4 (left). Overall the results fit in a good range for high undercooling and below 80 % conversion. For higher crystallization temperatures the fit is inadequate for conversions above 60 % with a decreasing trend. This is due to the two linear sections illustrated by the double logarithmic plot. Nevertheless the data was used to calculate the activation energy E_A whereas the results of 172°C and 173°C are not taken into account to have a direct comparison to the results calculated from peak times.

The activation energy was then calculated from the slope of a linear plot of $1/n \ln k$ and $\ln t_0$ respectively versus the reciprocal temperature, Fig. 4 (right).

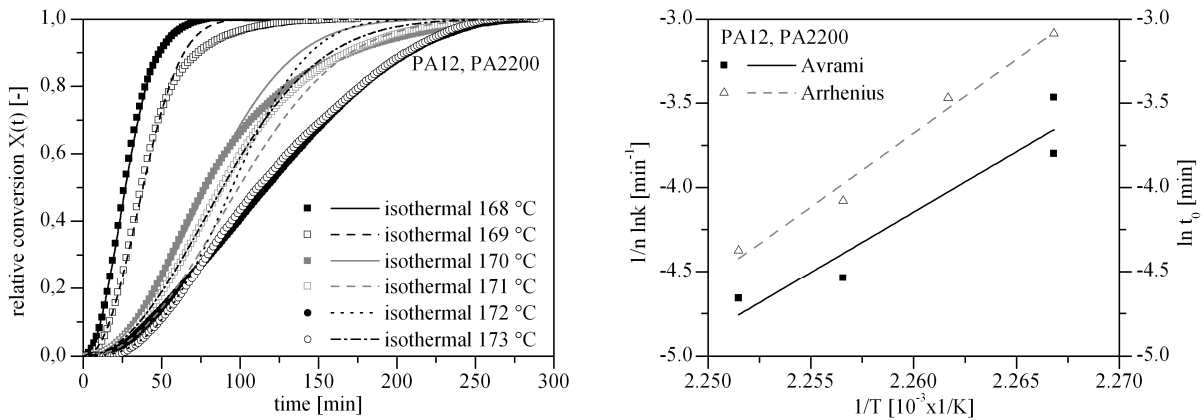


Fig. 4: Calculated and measured conversions (left) and fit curves to determine activation energies (right)

In Table 2 the results are shown for different polymers. Summing up the calculated activation energies the trend is comparable for both methods.

Material/Method	E_A [kJ/mol]	Material/Method	E_A [kJ/mol]
Method 1: Peak time		Method 2: Avrami	
PA12	$578,4 \pm 69,8$	PA12	$598,2 \pm 131,1$
PP	$265,0 \pm 24,2$	PP	$298,5 \pm 33,1$
POM	$1057,9 \pm 41,0$	POM	$1107,3 \pm 84,0$
PE-HD	$729,0 \pm 66,1$	PE-HD	$588,2 \pm 70,0$

Table 2: Comparison of the crystallization activation energy of multiple polymers achieved with the different methods investigated

Upon closer inspection the results show that POM and the investigated PE-HD have the highest activation energies. Thus, the gradient for the function describing the phase transformation due to crystallization is the highest in the measured temperature interval. On the other hand, PP and PA12 have the lowest slope and activation energy. Consequently a temperature change (undercooling) near the crystallization temperature is not as severe for the beginning and the overall kinetics of crystallization for PP and PA12. For the SLS process this has a severe influence on the tendency to curl when a new contour is molten and a new, slightly colder, layer of powder is applied. Subsequently this is a good indication of the robustness of new polymers for processing before broad studies on powders are conducted in SLS machines.

3.2 Simulation of thermal conditions in the building chamber

As shown before the temperature gradients while processing have a high influence on the crystallization the thermal conditions after penetration by a laser beam was studied more into detail. For basic studies on the thermal effects in a single layer the building process of a one line (length 10 mm, scan speed $v_s=1,0$ m/s) was simulated with various process parameters. Four points of the mesh (Fig. 1) were selected and their time and place dependent temperature curve is analyzed, Fig. 5. Thereby point 2 represents the surface temperature, point 8 the heat penetration depth and point 1 or 6 the width of the heat-affected zone on the surface as well in the volume.

Especially the surface temperature shows a severe influence by the kind of heat source. The surface heat source (1) results in a very high surface temperature. In contrary the volume heat source (-1) results in a more homogenous temperature distribution over the whole layer thickness (also on point 8). Hence the surface heat source causes a heat accumulation next to the surface due to the low heat conductivity of the polymer powder.

The volume heat source penetrates into the material and distributes the heat over the penetration length. Due to this fact the temperature at the points 6 and 8 are higher for the volume heat source compared to the surface heat source.

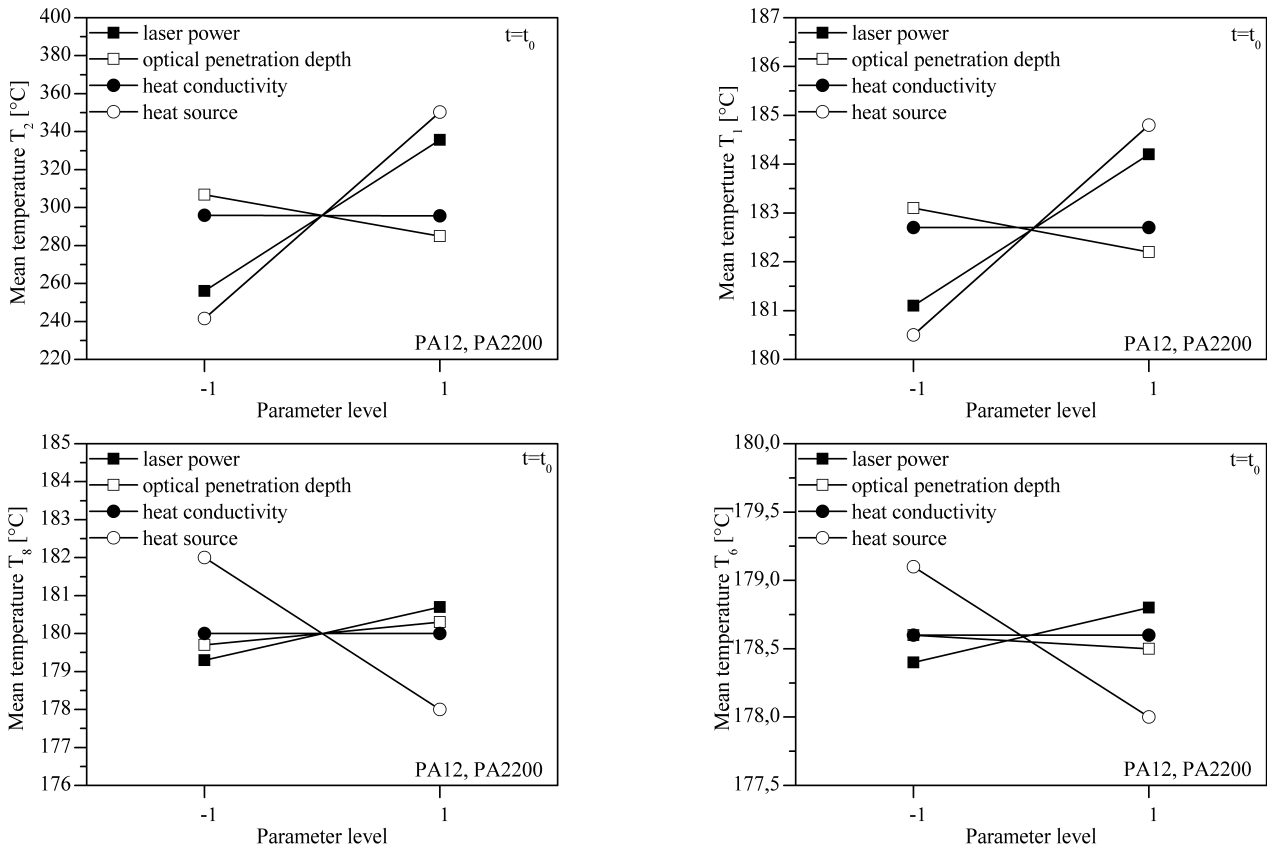


Fig. 5: Influencing parameters on the mean temperature at different points while penetration

Following effects on the temperature penetration depth can be identified exemplarily:

Laser power: An increasing laser power results in a higher heat penetration depth. Thus a higher heat flow (given that the optical penetration depth is constant) is measurable at the bottom of the layer.

Particle diameter / optical penetration depth: An increase of the particle diameter results in a higher optical penetration depth and higher sintering depths. Bigger particles cause exceeded cavities between the particles. Thus a higher penetration depth of the laser and consequently a higher temperature at the bottom of the layer is measured.

Thermal conductivity: No effects are visible, due to the high scan speed of the laser. Thus there is not enough time to transport heat by conduction.

Heat source: The temperature at the layer bottom decreases with the change from a volume to a surface source. The optical penetration by a volume source causes a homogenous temperature distribution over the penetration depth; in contrast to the surface source, which causes hot spots by slow heat conduction. Consequently the heat penetration depth during the laser penetration time is much more affected by optical effects than conduction effects for polymers.

To analyze the time dependent thermal effects at the chosen points, the temperature was calculated after the scanning time for a line (t_{line}). Fig. 6 shows the difference between the temperatures at the laser penetration time t₀ and after t_{line}.

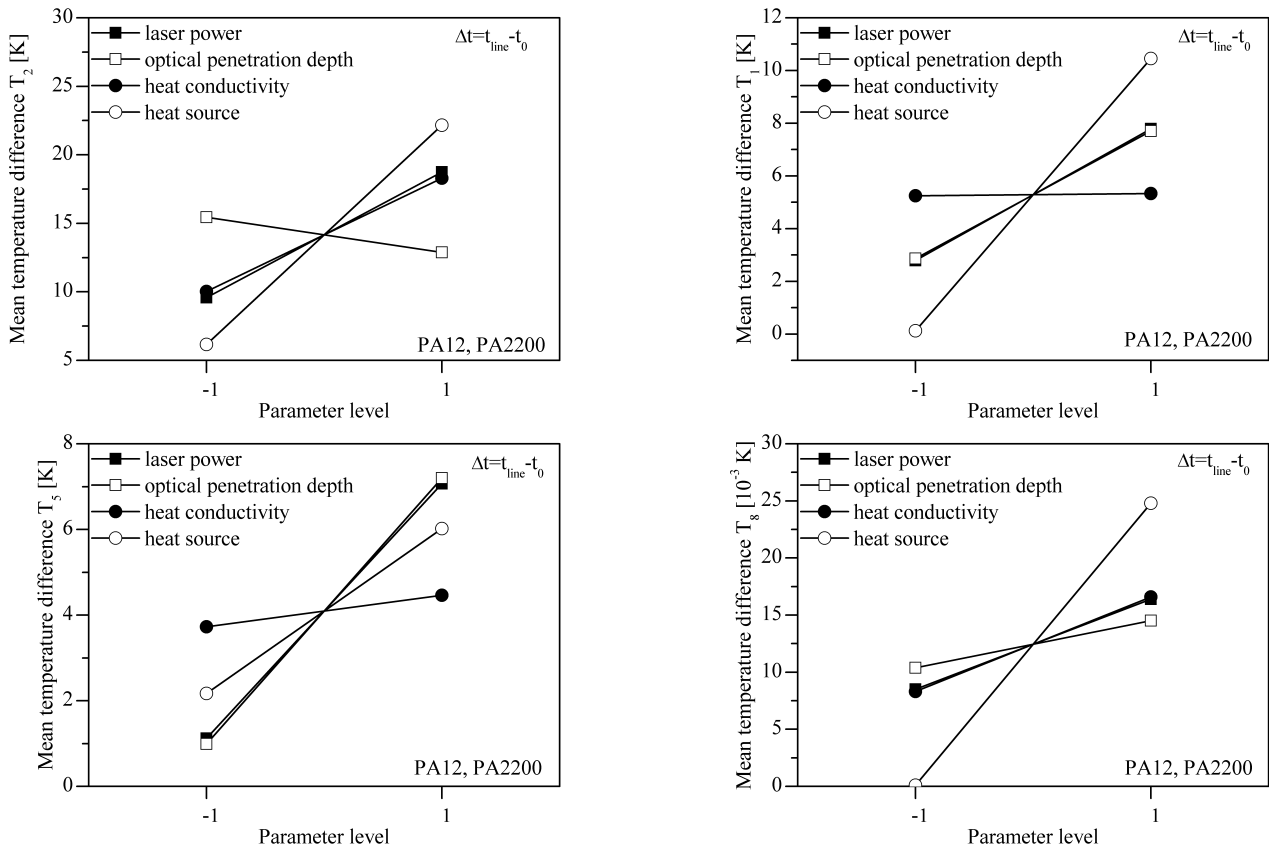
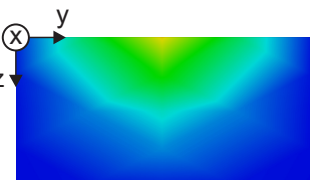

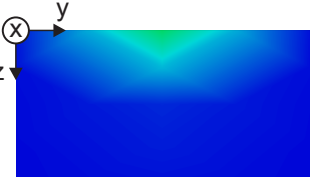


Fig. 6: Influencing parameters on the mean temperature at different points after the scanning time for one line

The maximum temperature difference is located near the molten surface. Reason therefore are thermal surface heat flows (e.g. radiation to the building chamber, free convection) pending on the surface. Monitoring the temperature difference at points deeper in the powder layer, it can be seen that the difference decreases. Hence inserted heat energy in deep layer regions is isolated by the surrounding powder (low conductivity level). Moreover the surface heat flows can't affect the deeper powder regions and conductivity isn't fast enough to cause a strong effect on the temperature difference, e.g. when a new layer is applied.

Due to the fact that optical parameters like the penetration depth or the absorbance of a powder are the major affecting parameters on the temperature distribution another reduced DoE was designed to study the optical effects detached from other boundary effects, Table 3.

Temperature distribution over a single layer	Parameters		Temperature [°C]
	Absorbance	66 %	
	Absorption coefficient	1/50 (1/μm)	
	Absorbance	33 %	
	Absorption coefficient	1/50 (1/μm)	

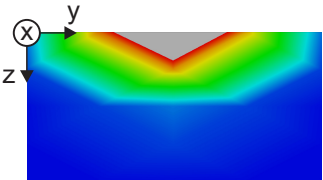
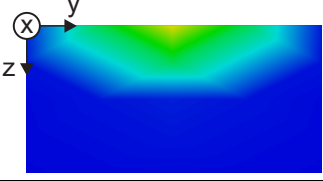
	Absorbance	66 %
	Absorption coefficient	1/25 (1/μm)
	Absorbance	33 %
	Absorption coefficient	1/25 (1/μm)

Table 3: DoE and simulation results of different optical parameters

Alike the first DoE an investigation of the temperature distribution on points 1, 2, 6, 8 during the laser penetration was done (Fig. 7).

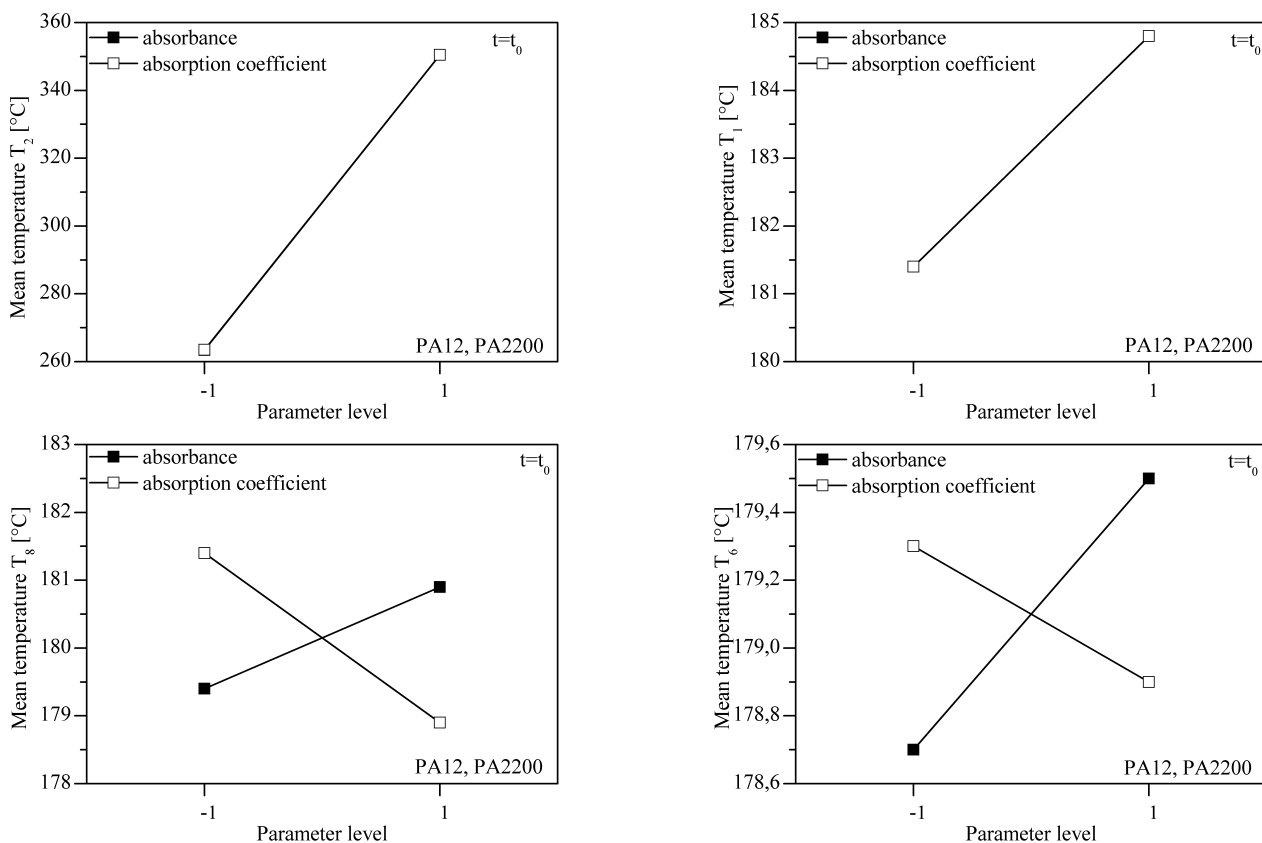


Fig. 7: Influencing optical parameters on the mean temperature at different points while penetration

Following effects of varying optical parameters on the temperature penetration depth can be identified exemplarily:

Absorbance: An increase of the absorbance results in a deeper heat penetration depth. An enlarged absorbance is similar to an increase of the laser power, as more laser energy is inserted into the powder.

Absorption coefficient / penetration depth: A decrease of the penetration depth or an increase of the absorption coefficient respectively causes a decrease of the heat penetration depth. A minor penetration depth results in a decrease of the penetration of the laser into the material, when prescribed effects are considered.

3.3 Correlations between scanning strategy and layer bonding

Besides the sole description of temperature fields the simulation is also a good tool to study the effects between scanning strategy and layer bonding. According to the simulation results for scanning a single line it can be concluded that the energy coupled into the polymer powder is well described by a volume heat source. The energy insertion of this heat source can then be affected by its parameters scanning speed and laser power. For typical parameters of a DTM Sinterstation 2000 this was calculated (Fig. 8) and compared with real temperature fields, measured with an infrared camera (Fig. 9).

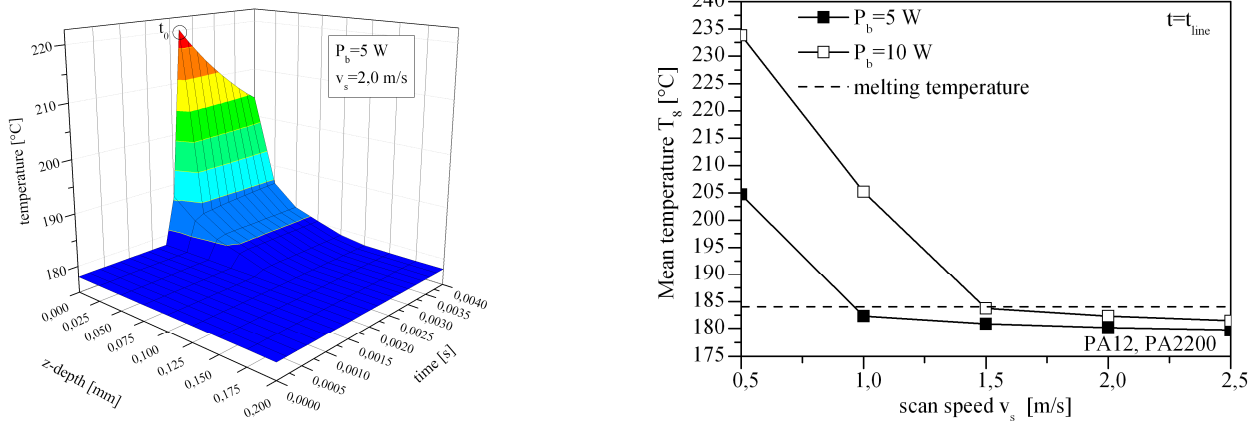


Fig. 8: Mean temperature distribution into the powder (left) and influence of scanning parameters on the temperature at point 8 ($z=100 \mu\text{m}$)

It can be seen that the top surface of the layer cools down very fast after the laser penetration at t_0 . In deeper regions the heat conduction from the surface to the layer bottom is insignificant due to isolation effects. Consequently the temperature at deeper points increases a little bit at the beginning and subsequently decreases slow with time. The findings of the simulated temperature fields agree well with effects that can be seen from experiments.

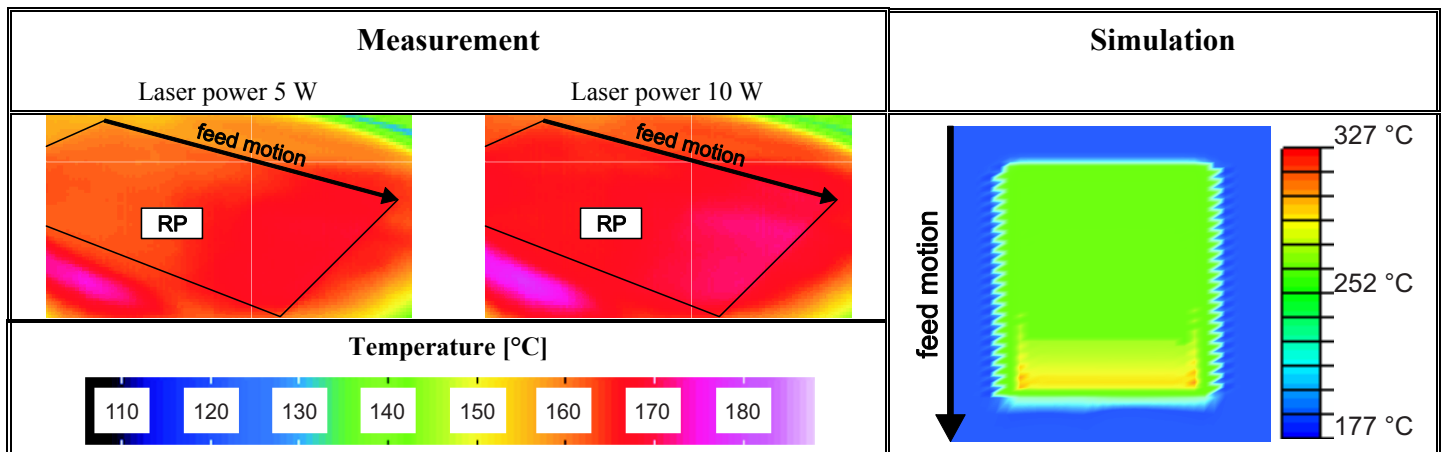


Fig. 9: Verification of simulation results (right) with experimental data of thermographs after applying a new layer onto a molten area (left)

4 Conclusion

In this paper it could be shown that the phase transition by means of crystallization of polymers is a highly time- and temperature-dependent process. Especially when new polymers should be processed there can be serious differences in the activation energy which can lead to untimely shrinkage and curl while a layer is scanned or when a new layer is applied. It can also be seen, that the simulation is able to depict both the local and the time

dependent temperature distribution. Especially the local temperature distribution by the scanning strategy is comparable with thermographs in the feed motion direction.

In conclusion it can be assessed, that the determinant parameter on the temperature distribution during the penetration of the material by the laser is the optical behavior of the powder. In opposition to this result, the heat conductivity of a polymer powder is in consideration of the low level of heat conductivity of polymers not an important parameter during the laser penetration. Reason for this behavior is that the inserted laser energy is seriously higher than every other heat flow in the powder or from the powder to the ambience. With rising process time the heat conductivity of the polymer powder has an increasing influence on the temperature distribution. Those findings can lead to new descriptions of the known curl effect and methods to avoid them, e.g. by different scanning strategies. By means of predicting mechanical and geometrical properties these simulated temperature fields can furthermore be used to simulate the crystallization process and the resulting degree in crystallinity.

5 Acknowledgements

The authors would like to thank the DFG for funding this research work in the SFB 814 “Additive Manufacturing” subproject B3.

Literature

1. Alscher, G., *Das Verhalten teilkristalliner Thermoplaste beim Lasersintern*. 2000, Universität Essen: Aachen.
2. Podszun, W., et al., *Verfahren und Material zur Herstellung von Modellkörpern*. 1999, Bayer AG: Deutschland.
3. J.-P. Kruth, et al., *Consolidation phenomena in laser and powder-bed based layered manufacturing*. p. 1-31.
4. Nöken, S., *Technologie des Selektiven Lasersinterns von Thermoplasten*, in *Fakultät für Maschinenwesen*. 1997, Rheinisch-Westfälische Technische Hochschule Aachen.
5. Eyerer, P., et al., *Rapid Prototyping - Neue Verfahren zum schnellen Herstellen von Prototypen*. *Kunststoffe*, 1993. **83**: p. S. 949 - 955.
6. Schmachtenberg, E., M. Schoenfeld, and T. Seul, *Material optimization of PA12 laser-sintering powder to improve surface quality*, in *Antec 2006*. 2006, Society of Plastic Engineers: Charlotte.
7. Rietzel, D., et al., *New Thermoplastic Powder for Selective Laser Sintering*. *Kunststoffe International*, 2008. **98**(2): p. 42-45.
8. Meyer, K.-R., et al., *Verfahren zur Herstellung von pulverförmigen Beschichtungsmitteln auf der Basis von Polyamiden mit mindestens 10 aliphatisch gebundenen Kohlenstoffatomen pro Carbonamidgruppe* 1979.
9. Monsheimer, S., et al., *Polymerpulver mit Polyamid, Verwendung in einem formgebenden Verfahren und Formkörper, hergestellt aus diesem Polymerpulver*, E. Patentamt, Editor. 2009.
10. Lynch, A.J. and C.A. Rowland, *The history of grinding*. 2005: Society for Mining, Metallurgy, and Exploration.
11. Drummer, D., D. Rietzel, and F. Kühnlein, *Development of a characterization approach for the sintering behavior of new thermoplastics for selective laser sintering*. *Physics Procedia*, 2010. **5**(Part 2): p. 533-542.
12. Lorenzo, A.T., et al., *DSC isothermal polymer crystallization kinetics measurements and the use of the Avrami equation to fit the data: Guidelines to avoid common problems*. 2006: p. 222-231.
13. Minying, L., et al., *Melting behaviors, isothermal and non-isothermal crystallization kinetics of nylon 1212*. 2002: p. 1 - 9.
14. J. Sestak and G. Berggren, *Study of the kinetics of the mechanism of solid-state reactions at increasing temperatures*. *thermochimica acta*, 1971. **3**: p. 1-12.
15. Tontowi, T.H.C.C.a.A.E., *Selective laser sintering of a crystalline and a glass-filled crystalline polymer: experiments and simulations*. School of Mechanical Engineering, University of Leeds, UK, 2001. **215 Part B**: p. 15.
16. Rietzel, D., F. Kühnlein, and D. Drummer, *Characterization of New Thermoplastics for Additive Manufacturing by Selective Laser Sintering* SPE Proceedings ANTEC, 2010.
17. Keller, B., *Grundlagen zum selektiven Lasersintern von Polymerpulver*. Dissertation. 1998: Universität Stuttgart.
18. Steinberger, J., *Optimierung des Selektiven-Laser-Sinterns zur Herstellung von Feingußteilen für die Luftfahrtindustrie*. Verein Deutscher Ingenieure: [Fortschrittberichte VDI / 2]. 2001, Düsseldorf: VDI-Verl.
19. Liu, M., et al., *Melting behaviors, isothermal and non-isothermal crystallization kinetics of nylon 1212*. 2003: p. 1 - 9.